Ligament and Droplet Characteristics in Prefilming Airblast Atomization

S. Gepperth[*1], A. Müller[2], R. Koch[1] and H.-J. Bauer[1]
[1]Institut für Thermische Strömungsmaschinen, Karlsruher Institut für Technologie (KIT), Karlsruhe, Germany
[2]Lechler GmbH, Metzingen, Germany
sebastian.gepperth@kit.edu and armin.mueller@lechler.de

Abstract

Liquid film breakup of three different geometrical variants of a planar prefilming airblast atomizer have been studied using advanced Particle Tracking Velocimetry (PTV) coupled with ligament tracking. In addition to the variation in geometry, liquids with different physical properties (surface tension, viscosity) have been tested. The liquid mass flow rate and mean air velocities were varied over a wide range of test conditions. A post-processing algorithm was developed to capture the ligament and droplet sizes and their velocities. For the test conditions investigated, it was observed that the mean air velocity and the thickness of the atomizing edge are the key parameters that influence the breakup process. From the database of test cases, correlations for the ligament breakup frequency, Sauter mean diameter and mean velocity of the primary droplets are derived.

Introduction

Nowadays, in modern aviation no real alternatives to gas turbine engines exist. Therefore, a continuing development in this sector is inevitable. In addition to the reliability and safety of those engines, the key focus is on the reduction of green house gas emissions. Due to stricter regulations in aviation, a continuing reduction of NO_x, CO_x and unburned hydrocarbons in those engines is essential. One solution to this can be the reduction of the specific fuel consumption. The other possibility is to use lean combustor strategies. Those combustors operate below the stoichiometric fuel to air ratio and produce low emissions.

Prefilming airblast atomizers are widely used for fuel injection in such gas turbine engines and have a number of advantages including fine atomization, comparatively little change in performance over a wide range of fuel flow rates, and low pressure losses [11].

Many previous studies of airblast atomizers have been performed using actual atomizers at various test conditions [1, 5 and 13] or simplified planar injectors. In most cases, the simplified geometries investigated were of the non prefilming type. Those atomizers eject a planar liquid sheet at the atomizing edge that then disintegrates into isolated structures [4, 6 and 7]. However, little research on prefilming airblast atomizers is currently available that includes information of the ligaments and droplets generated close to the atomizing edge [2 and 8] and the mechanisms and processes leading to film disintegration and spray generation are not fully understood. Therefore, new designs of such atomizers are developed using costly experimental trial and error.

To address this problem, detailed measurements of the liquid film breakup process have been performed. The experimental results will help to gain a better understanding of the atomization process as well as to create a large database of experimental results. Based on this database, correlations are derived to predict the initial droplet properties for prefilming airblast atomizers. On the other hand, numerical simulations for the liquid film breakup can be calibrated and validated against these experimental results.

Experimental Setup

The measurements have been conducted at the spray test rig at the Institut für Thermische Strömungsmaschinen (ITS). The air is supplied by a radial compressor with a maximum mass flow of 200g/s. The air mass flow is measured via an air mass flow meter. To ensure a homogeneous velocity field, a system of mixer, flow straightener and a nozzle is positioned upstream of the test section. To capture the relevant flow parameters, pressure and temperature probes are connected to the mixing unit.

In order to enhance the optical accessibility, the test section itself (Figure 1) is a two-dimensional abstraction of an axis-symmetric airblast atomizer. It consists of four wall segments and the prefilming surface. The air emerging from the mixer is split into two air streams that pass the prefilmer on each side.

Inside the prefilmer a cavity is located, which is used as a continuous feed for the test liquids. The liquid is ejected through a set of 50 equidistant distributed holes with a diameter of 0.5mm each. The air shear causes the liquid to form a uniform thin film flowing in the *Z*-direction. It was ensured that no film dry-out was occurring during the experiments. The liquid flow through the test section is controlled by a mass flow meter/controller. All experiments were performed at ambient conditions. The operating conditions are summarized in Table 1.

To investigate the effect of different liquid properties on the liquid film breakup and the resulting droplets, a total of six different liquids were used for the spray experiments. Those liquids cover the possible range of liquid

* Corresponding author: sebastian.gepperth@kit.edu

properties of Jet-A1 during flight conditions. However, additional liquids were used to gain a better understanding of the role of viscosity and surface tension during liquid film breakup. The relevant physical properties of the liquids used for the experiments are listed in Table 2.

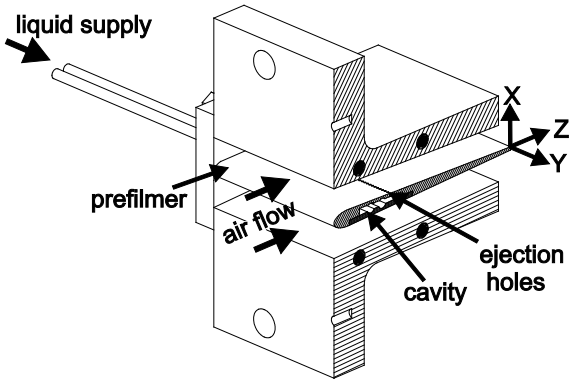

Figure 1: Schematic of the test section

Table 1: Operating conditions

mean air velocity	$\overline{u_g}$	20 – 70 m/s
air temperature	T	298 K
air density	ρ	1.21 kg/m³
air kinematic viscosity	ν	1.5×10^{-5} m²/s
volumetric liquid film flow rate	$\dot{V}/b$	12.5 – 75 mm²/s

Table 2: Physical properties of investigated liquids

	density	**kinematic viscosity**	**dynamic viscosity**	**surface tension**	**temperature**
	ρ_l	ν_l	μ_l	σ_l	T_l
	[kg/m³]	**[m²/s]**	**[kg/m·s]**	**[kg/s²]**	**[K]**
Shellsol D40	742.0	1.09×10^{-6}	0.812×10^{-3}	0.0255	298
Shellsol D60	767.0	1.63×10^{-6}	1.25×10^{-3}	0.0268	298
Shellsol D70	770.0	2.03×10^{-6}	1.56×10^{-3}	0.0275	298
Shellsol D100	777.0	3.02×10^{-6}	2.34×10^{-3}	0.0283	298
1,2-Propanediol	1021.0	52.2×10^{-6}	53.3×10^{-3}	0.0381	298
1:1 vol. mix.: H_2O-1,2-Pro.	1008.0	6.01×10^{-6}	6.06×10^{-3}	0.0466	298

Prefilmer Configurations

For all tested configurations, planar prefilmers have been used. Figure 2 shows the most important geometrical parameters. The channel heights as well as the length upstream of the liquid film injection have been kept constant for all three configurations. The duct has a wide aspect ratio to avoid any interference between the corner vortices and the liquid film ejected in the middle section of the prefilming surface. All prefilmer configurations as well as the walls of the test section have been manufactured of Perspex for better optical access.

Three different prefilmer configurations have been tested in order to study the effect of varying prefilming length *l* and atomizing edge thickness *h*. By changing one of these two parameters, the corresponding other parameters were adjusted accordingly to maintain an unchanged velocity field. The characteristic parameters of the investigated atomizers are listed in Table 3.

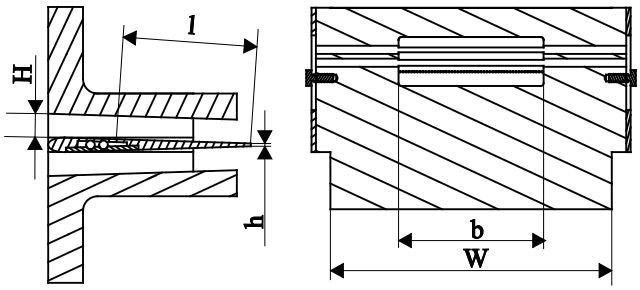

(a) *XZ*-plane (b) *YZ*-plane

Figure 2: Definition of geometrical parameters

Table 3: Investigated geometry parameters

prefilming length	l	20.6 mm, 47.6 mm
atomizing edge thickness	h	1.0 mm, 2.5 mm
prefilming width	b	50 mm
air channel height	H	8.11 mm
air channel width	W	96 mm
prefilmer chord length	L_C	43.1 mm, 70.9 mm

Diagnostics

For the detailed investigation of the liquid film atomization process, a combined method of particle and ligament tracking velocimetry has been used. The technique is based on backlight illumination of a measurement volume (shadowgraphy) with a double-pulsed laser. The field of view is 12 mm in the *Z*-direction and 16 mm in the *Y*-direction. The spatial resolution is 10 µm. Details on the optical setup and the measurement system can be

found in the paper of Gepperth et al. [8]. The key advantage of this technique is that information about the accumulated liquid at the atomizing edge and the generated droplets are gathered at the same time. This helps to link the produced droplets near the atomizer edge to the deformation of the liquid accumulation at the atomizing edge by which the droplets are generated.

The software for the post-processing has previously been developed at ITS [9 and 12]. The post-processing routine can be divided in four major tasks. First, a grey scale analysis of the recorded double frame images is performed. In the second step, a contouring algorithm is applied. This algorithm detects connected structures based on the grey scale level. It further divides the detected areas into the accumulated liquid at the atomizer edge and droplets. After that, the accepted droplets are corrected in size by a depth-of-field (DoF) correction based on the results presented in [14 and 15]. This correction leads to a significant increase in the measurement accuracy.

The third step is the calculation of the droplet velocities in the *YZ*-plane, based on the displacement of each droplet and the interframing time between two images. In the last step, the geometrical parameters of the accumulated liquid are recorded. The yellow line in Figure 3 indicates the perimeter of the accumulated liquid, P_{str}. The red dots along the perimeter represent the maximum elongation of the liquid accumulation in the streamwise direction. Based on the atomizing edge and the detected maxima, the breakup length of the ligaments, L_{str} can be derived. The last measured characteristic of the accumulated liquid is the covered area, A_{str}. It is defined as the area between the atomizing edge and the perimeter of the accumulated liquid that is covered by the liquid.

In addition, the detected liquid accumulation at the atomizing edge of subsequent temporal frames is used to calculate the stream wise deformation velocity $u_{def,\,str}$ of the liquid.

For each test case a set of 300 double frame images (approx. 2.000 to 200.000 droplets) was post-processed.

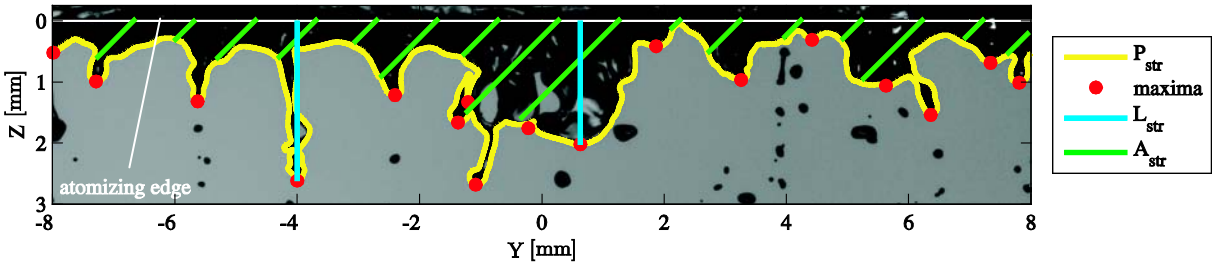

Figure 3: Definition of the geometrical parameters of the accumulated liquid

Measurement Uncertainty

The measurement uncertainty has been determined using the approach given by Kline and McClintock [10]. The uncertainty in setting the mean air velocity can be estimated to 3%. The uncertainty for the liquid mass flow is less than 0.5%. Due to the enhanced calibration and post-processing system, the error in measuring the droplet size and velocity is estimated to be less than 4%. In summary, the maximum uncertainties for the measurements are about 7%.

Results and Discussion

During the experimental investigations, it was observed that the breakup process always consists of the same three stages (Figure 4). First, a reservoir is formed at the atomizing edge. Second, "bubble" like ligaments are formed out of this reservoir. As soon as this "bubble" bursts, small droplets are produced. The rim of the "bubble" remains attached to the reservoir and disintegrates later into larger droplets.

(a) $\overline{u_g} = 20\ m/s$ (b) $\overline{u_g} = 50\ m/s$ (c) $\overline{u_g} = 70\ m/s$

Figure 4: Effect of mean air velocity on liquid accumulation (Shellsol D70, $\dot{V}/b$ = 25 mm²/s)

Effect of air velocity and liquid properties on ligament formation

First, the effects of mean air velocity and liquid properties on the atomization process are discussed. Increasing the air velocity reduces the length of the observed ligaments. A change in liquid properties shows the same effect. With higher surface tension the ligaments grow larger before disintegration.

When comparing the mean area to perimeter ratio of the accumulated liquid $\overline{A_{str}}/\overline{P_{str}}$ (Figure 5 a) as function of mean air velocity, a distinct tendency is visible. It can be seen that $\overline{A_{str}}/\overline{P_{str}}$ decreases with increasing air velocities. Based on the area and perimeter data as well as the raw images, it can be concluded that the number of atomization events increases with increasing air velocities. However, the larger number of these events seems to have no influence on the area whereas the perimeter increases at the same time and, therefore, $\overline{A_{str}}/\overline{P_{str}}$ decreases. As mentioned before, a higher liquid viscosity and surface tension leads to larger ligaments. Thus, for a constant air velocity, $\overline{A_{str}}/\overline{P_{str}}$ is increasing when increasing viscosity and surface tension.

When investigating the mean length of the examined liquid accumulation, $\overline{L_{str}}$ (Figure 5 b) it is obvious that increasing air velocity slightly reduces the breakup length. The larger deviations at low air velocities are due to large structures that exceed the field of view and lead to erroneous measurements, as indicated by the error bars. The error bars in Figure 5, 7 and 9 represent the standard deviation around the mean value. The reduction in breakup length seems reasonable if it is taken into account that an increase in air velocity induces higher aerodynamic forces. Those forces act on the stretched ligaments and cause them to be destabilized faster and thus lead to earlier fragmentation. On the other hand it is well known, that higher surface tension and viscosity tend to stabilize a liquid structure, which leads to an increased ligament length.

In addition to the geometrical parameters of the accumulated liquid, Figure 5 (c) shows the measured streamwise deformation velocity of the accumulated liquid, $\overline{u_{def,str}}$. A linear increase with increasing air velocity is noticeable. This increase is due to the increase in aerodynamic forces acting on the liquid surface. Shear forces caused by the faster air stream accelerate the liquid surface near the atomizer edge. Both, the deformation velocity (Figure 5 c) and the breakup length (Figure 5 b) of the liquid accumulation show a noticeable tendency to shorter length and faster deformation, regardless of the physical properties of the liquid. When combining L_{str} and $u_{def,str}$ a breakup frequency: $f_{breakup} = u_{def,str}/L_{str}$ can be calculated. The mean breakup frequency, $\overline{f_{breakup}}$ (Figure 5 d) is a measure for the time distance between consecutive atomization events and shows a linear increase with increasing mean air velocity. The liquid properties do not change this linear behavior but affect the absolute value of the breakup frequency due to the stabilizing effects of higher viscosity and surface.

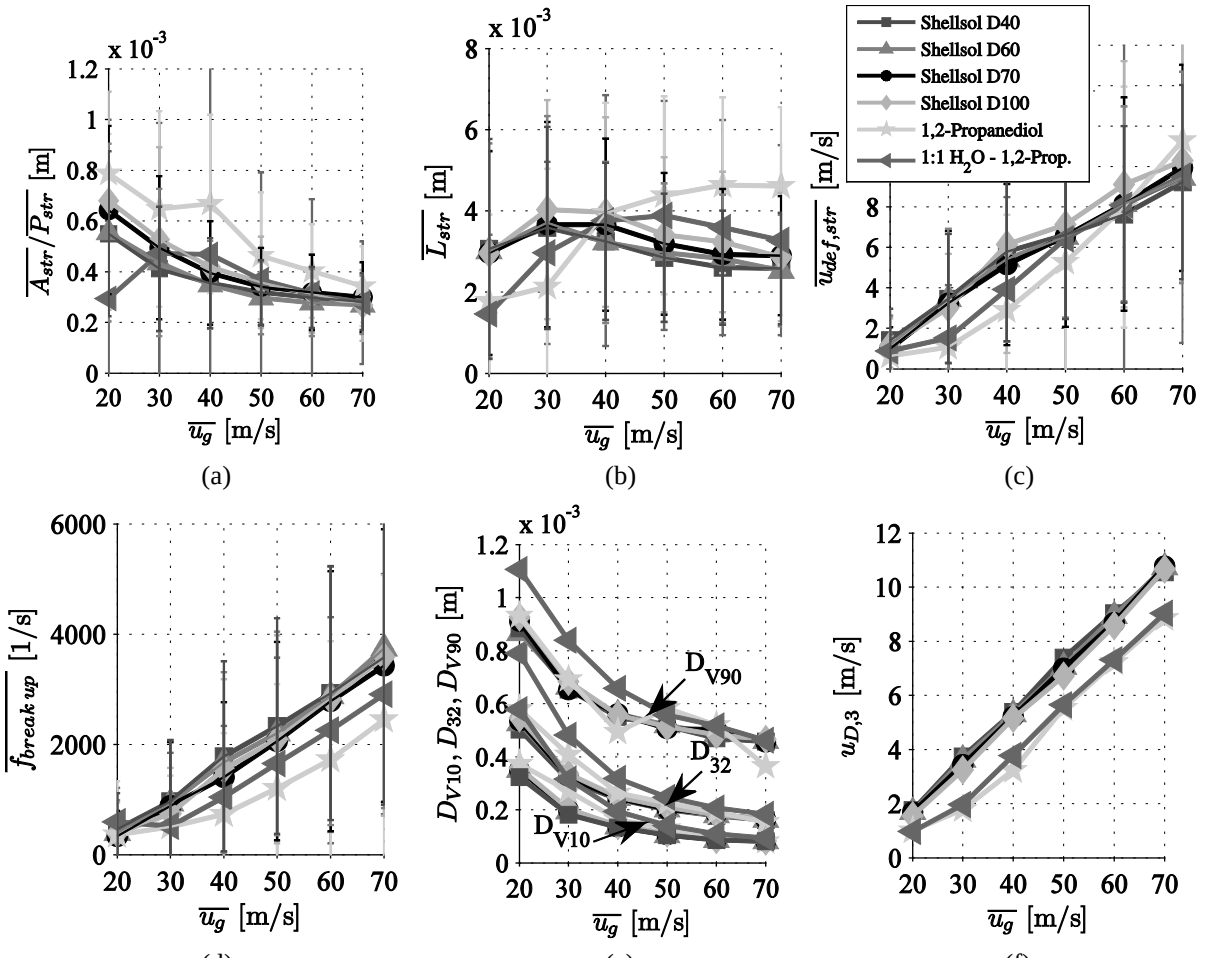

Figure 5: Effect of mean air velocity and liquid properties on the breakup process (a) to (d) and the generated droplets (e, f) ($\dot{V}$/b = 25 mm²/s)

Effect of air velocity and liquid properties on droplet size and velocity

With the previously explained diagnostics, it was possible to measure droplet sizes and velocities simultaneously. In Figure 5 (e) the change of the characteristic droplet diameter with increasing air velocity is presented. The curves in the upper section of the graph represent the D_{V90} and give an indication on the upper size range of the droplets produced during the fragmentation of the liquid film. At the bottom of Figure 5 (e) are the curves that represent the lower bound of the produced droplets, D_{V10}. The curves in the middle of Figure 5 (e) represent the Sauter mean diameter (D_{32}). All diameters follow the same trend. They first drastically decrease with increasing air velocity and seem to converge to a level where a further increase in mean air velocity will only have a minor effect on the droplet diameters. This result can be explained by a closer look to the flow field at the atomizer edge. A higher mean air velocity leads to a reduced wake downstream of the atomizing edge. Therefore, the droplets are exposed to a higher aerodynamic loading earlier and will be fragmented. If the air velocity is gradually increased, the droplets are atomized within the observed field-of-view and reach a stable size. This means, that only a significant increase in mean air velocity, beyond the investigated conditions, will lead to an atomization of these small droplets.

Figure 5 (f) shows the volume weighted mean droplet velocity $u_{D,3}$as a function of the mean air velocity: $u_{D,3} = \sum_{i=1}^{N} u_i \cdot D_i^3 / \sum_{i=1}^{N} D_i^3$. It is observed that $u_{D,3}$ linearly increases with increasing mean air velocity. The liquid properties also have an effect on the mean droplet velocity. Higher surface tension and liquid viscosity lead to lower droplet velocities. The highly viscous liquids remain attached to the atomizer longer (Figure 5 b). In consequence, the separated droplets are exposed later to the air flow and, thus their velocity is lower. In addition, the liquids with higher viscosity and surface tension produce larger droplets. Based on the larger inertia of those droplets they need more time to be accelerated up to the air flow velocity and, therefore, have a lower velocity within the measurement area. It can be concluded that those slow and large droplets will be further atomized as they move away from the atomizer edge.

For a combustion chamber, the large droplets are crucial. Due to their low velocity and huge mass, those droplets will not perfectly follow the air flow and, therefore, have a significant effect on the spray propagation and fuel distribution. This will have an impact on the emissions and stability of the flame.

Effect of liquid loading

Details of the effect of liquid loading on the atomization process and the produced droplets are illustrated in Figure 6. The visual inspection showed only a little effect of the liquid loading on the size and structure of the single ligaments. The number of atomization events on the other hand and, therefore, the number of droplets produced is increasing, with increasing liquid mass flow.

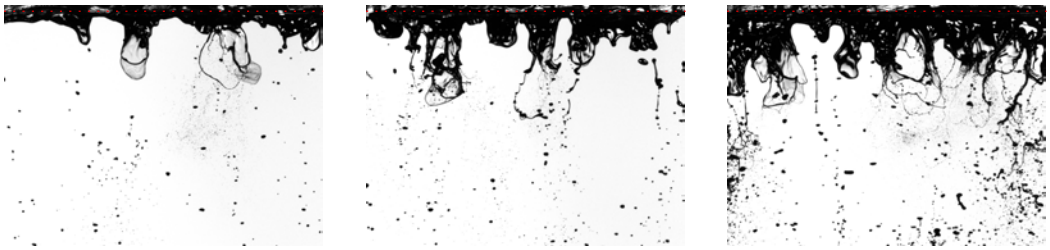

(a) $\dot{V}/b$ = 25 mm²/s (b) $\dot{V}/b$ = 50 mm²/s (c) $\dot{V}/b$ = 75 mm²/s

Figure 6: Effect of liquid loading on liquid accumulation (Shellsol D70, $\overline{u_g}$ = 60 m/s)

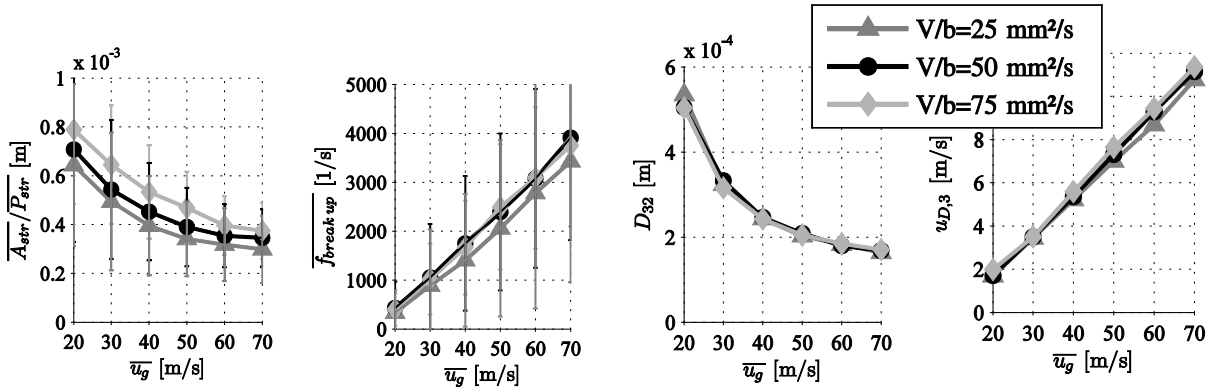

(a) (b) (c) (d)

Figure 7: Effect of liquid loading on the breakup process (a, b) and the generated droplets (c, d) (Shellsol D70)

The measured area to perimeter ratio (Figure 7 a) indicates the same behavior for all investigated liquid loadings. For a constant air velocity, an increase in liquid loading leads to a linear increase of $\overline{A_{str}}/\overline{P_{str}}$. This

tendency was found for all tested liquids. When looking at $\overline{f_{breakup}}$ (Figure 7 b), only a small variation with increasing liquid loading was found. The breakup frequency is slightly increasing for an increased liquid loading from 25mm²/s to 50mm²/s, but then no further change can be observed. The comparison of the area to perimeter ratio and the breakup frequency together with the visual observations (Figure 6) leads to the conclusion that the liquid loading has no effect on the atomization process itself, but only affects the number of atomization events due to the increased liquid flow rate.

The characteristic droplet diameters and droplet velocities do not depend on the liquid loading at all (Figure 7 c and d). The droplet diameters and mean droplet velocities remain constant for all investigated conditions and liquids. The only difference is that, due to the increased liquid flow rate, the number of generated droplets is increased.

Effect of the prefilmer geometry

The last investigated parameter in this experimental study is a variation in prefilmer geometry, namely the wetted length of the prefilming surface and the thickness of the atomizing edge. Figure 8 shows a set of images for the investigated configurations. From those images, it can be concluded that the change in prefilmer length has no visual effect on the atomizing mechanism and ligament sizes. On the other hand, when comparing the 1mm atomizer edge (Figure 8 a) and the 2.5mm atomizer edge (Figure 8 c) a significant difference can be seen. The observed ligaments show a significant increase in size. In addition to the impact of these geometrical changes on the accumulated liquid, a significant change in the produced droplets is observed.

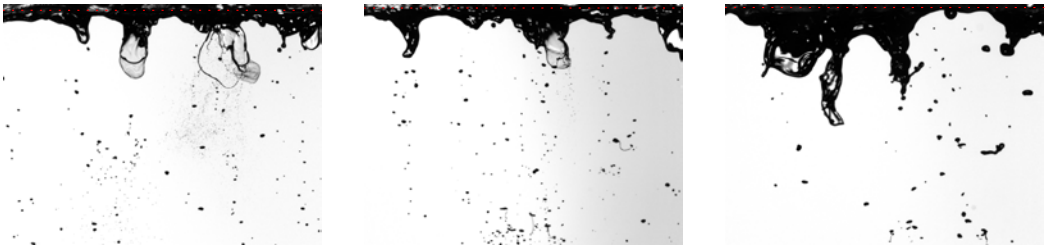

(a) h = 1 mm, l = 47.57 mm *(b)* h = 1 mm, l = 20.57 mm *(c)* h = 2.5 mm, l = 47.61 mm

Figure 8: Effect of pre-filming configuration on liquid accumulation (Shellsol D70, $\overline{u_g}$ = 60 m/s)

When comparing the area to perimeter ratio (Figure 9 a), only a small difference between the two investigated prefilmer length can be seen. $\overline{A_{str}}/\overline{P_{str}}$ is slightly increased for the shortened prefilmer. A more pronounced change of $\overline{A_{str}}/\overline{P_{str}}$ is observed for the variation in the atomizing edge thickness. $\overline{A_{str}}/\overline{P_{str}}$ is almost increased by 100% for all investigated conditions. The same effect is observed for the breakup frequency. The prefilmer length has no impact on $\overline{f_{breakup}}$ at low mean air velocities. Only for the highest investigated velocities a small reduction in $\overline{f_{breakup}}$ is observed for the short prefilmer. However, this difference is not fully understood and needs to be investigated further.

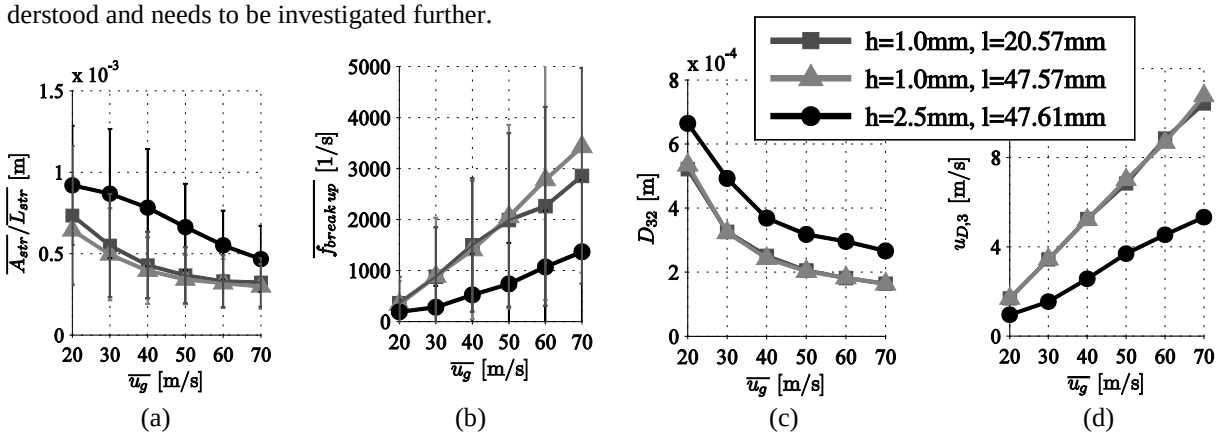

Figure 9: Effect of pre-filming length and atomizer edge thickness on the breakup process (a, b) and the generated droplets (c, d) (Shellsol D70, $\dot{V}$/b = 25 mm²/s)

On the other hand, the atomizing edge thickness seems to have a significant impact on the breakup frequency. $\overline{f_{breakup}}$ is reduced by 50% when comparing the results of the 2.5mm edge to the 1mm atomizer edge at the same mean air velocity. In conjunction with the visual observations, this leads to the assumption that the film flow itself is decoupled from the atomization process. Obviously, the liquid film flow is accumulated at the atomizer edge before it is disintegrated. Therefore, a larger liquid volume is stored at the thicker atomizing edge.

A comparison of the produced droplet sizes is shown in Figure 9 (c). The D_{32} is not affected by the reduced prefilmer length, whereas the increased atomizer edge thickness has a strong impact. For the same mean air

velocities D_{32} increases by almost 50% compared to the other two configurations. The volume weighted mean droplet velocity $u_{D,3}$ for the three investigated geometries are compared in Figure 9 (d). It is shown, as it was observed for the ligament characteristics, that only the atomizing edge thickness has a significant effect. For the 2.5mm atomizing edge, the generated droplets have a lower velocity compared to those of the 1mm atomizing edge. The produced droplets are larger and therefore, need more time to be accelerated by the air flow. At the same time, the thicker atomizing edge induces a larger wake region, where lower air velocities can be observed. Consequently, the generated droplets itself have lower velocities.

Correlations

For all conditions considered here the freestream turbulence level at the inlet of the test section was measured to be between 8% and 9%. Therefore, the turbulent boundary layer thickness at the atomizing edge was assumed by: $\delta_{x\,edge} = 0.16 \cdot L_C / Re_{x\,edge}^{1/7}$ [16]. This characteristic length scale was used to derive three characteristic non-dimensional numbers based on the experimental results presented and the approximately 300 test cases investigated: the Strouhal number, the non-dimensional Sauter mean diameter and the non-dimensional droplet velocity. In order to derive these numbers, a dimension analysis based on the Buckingham-π-theorem [3] has been performed.

To determine the time interval between subsequent breakup events the Strouhal number can be used $Sr_{f,breakup} = \overline{f_{breakup}} \cdot h/\overline{u_g}$. The best fit between measurements and predictions could be obtained by:

$$Sr_{f,breakup} = 3.7 \cdot 10^{-3} \cdot Re_\delta^{-0.51} \cdot We_\delta^{0.72} \cdot Oh_\delta^{-0.13} \cdot \left(\frac{\dot{V}/_b}{\overline{u_g} \cdot \delta_{x\,edge}}\right)^{0.14} \cdot \left(\frac{\rho_l}{\rho_g}\right)^{0.55}. \quad \textbf{(1)}$$

The agreement between the experimental results and the predictions by equation (1) is in general very good (Figure 10, a). Most of the predicted values are lying within 11% of the experimental results.

In order to characterize the droplet sizes generated by the breakup of the accumulated liquid, the non dimensional Sauter mean diameter:

$$D_{32}/\delta_{x\,edge} = 4.96 \cdot Re_\delta^{-0.17} \cdot We_\delta^{-0.36} \cdot \left(\frac{\rho_l}{\rho_g}\right)^{-0.013} \cdot \left(\frac{h}{\delta_{x\,edge}}\right)^{0.46} \quad \textbf{(2)}$$

is introduced. A very good agreement between measured and predicted Sauter mean diameter can be demonstrated for the investigated range of test conditions (Figure 10, b). The error is less than 6% in most cases. Only for the lowest air velocities, i.e. the upper range of Figure 10 (b), the deviation is higher (approx. up to 36%). This might be linked to a change in the atomization mechanism at very low mean air velocities.

For the correlation of the droplet velocity the volume weighted mean droplet velocity $u_{D,3}$ was divided by the mean air velocity. The following equation represents the best fit between measured and predicted data.

$$u_{D,3}/\overline{u_g} = 49.49 \cdot Re_\delta^{-1.83} \cdot We_\delta^{1.18} \cdot \left(\frac{\rho_l}{\rho_g}\right)^{0.52} \cdot \left(\frac{h}{\delta_{x\,edge}}\right)^{-0.8}. \quad \textbf{(3)}$$

Figure 10 (c) shows the comparison between predicted (Eq. 3) and measured droplet velocities. The error is in many cases within 10%. The deviation at the upper range of Figure 10 (c) is due to the fact, that the volume weighted mean droplet velocity in the wake region is limited by the air velocity in this region and not by the mean air velocity. This effect was not captured by the analysis performed here.

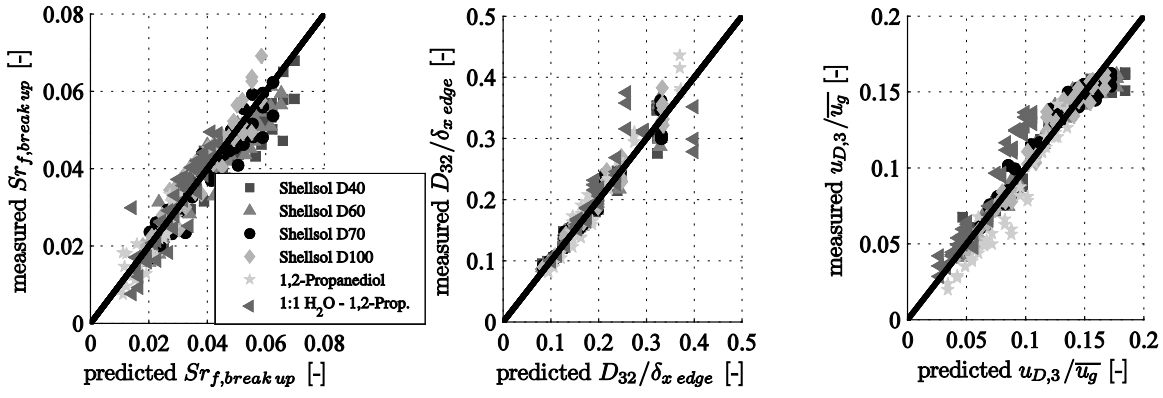

(a) (b) (c)

Figure 10: Comparison between measurements and predictions, (a) $Sr_{f,breakup}$, (b) non dimensional D_{32} and (c) non dimensional mean droplet velocity

Summary and Conclusions

The influence of liquid physical properties, air velocity, film flow rate, prefilming length and atomizing edge thickness on primary atomization were studied by means of a combined droplet and ligament tracking velocimetry system. Particular attention was paid to the characteristics of the accumulated liquid as well as to the droplet diameters and velocities.

For the range of test conditions studied, mean air velocity and atomizing edge thickness were found to be the dominating parameters. The prefilming length, liquid physical properties and liquid volume flow rate seem to have only a minor effect on the mean droplet diameter but affect the ligament formation process.

Based on the experimental results, a set of correlations is derived that can be used to predict the breakup frequency, Sauter mean diameter and mean droplet velocity in the primary breakup region of an airblast atomizer.

The work will be continued by similar measurements at elevated pressure. The results will then be included in the present correlations in order to cover the operating conditions of real gas turbines.

Acknowledgements

The research has been partially funded by the European Community's Seventh Framework Programme (FP7/2007-2013) under Grant Agreement n° ACP8-GA-2009-234009.

This study is part of the 4-year KIAI project which addresses innovative solutions for the development of new combustors in aero-engines. It aims at providing low NOx methodologies to be applied to design these combustors.

Nomenclature

Symbols

D	droplet diameter [m]	$Sr_{f,breakup}$	Strouhal number [-]
f	frequency [1/s]	δ	boundary layer thickness [m]
A	area of the liquid accumulation [m²]	D_{32}	Sauter mean diameter [m]
P	perimeter of the liquid accumulation [m]	$\dot{V}/b$	volumetric film flow rate per unit length, liquid loading [mm²/s]
L	length of the liquid accumulation [m]		
L_C	chord length of the atomizer [m]	**Subscripts**	
h	atomizing edge thickness [m]	g	gas
b	pre-filming surface wetted width [m]	l	liquid
D_{V90}	drop diameter such that 90% of total liquid volume is in droplets of smaller diameter [m]	*breakup*	disintegration of the liquid accumulation, breakup
D_{V10}	drop diameter such that 10% of total liquid volume is in droplets of smaller diameter [m]	*str*	liquid accumulation, liquid attached to the atomizing edge
$\bar{u}$	mean velocity through a *xy*-plane [m/s]	*def*	deformation
We_δ	Weber number, $\rho_g \overline{ug}^2 \delta_{x\ edge}/\sigma_l$ [-]	*D*	droplet/particle
Oh_δ	Ohnesorge number, $\mu_l/(\sigma_l\ \delta_{x\ edge}\rho_l)^{0.5}$ [-]	*3*	volume weighted
Re_δ	Reynolds number, $\rho_g \overline{ug} \delta_{x\ edge}/\mu_g$ [-]	*x edge*	position at the atomizing edge

References

[1] Beck, J. E. and Lefebvre, A. H., *Journal of Propulsion*, 7: 207-212 (1991).
[2] Bhayaraju, U. C., Giuliani, F. and Hassa, C., *ILASS Europe, 20th Annual Conference on Liquid Atomization and Spray Systems*, Orleans, France, (2005).
[3] Buckingham, E., *Physical Review*, 4: 345-376, (1914).
[4] Carvalho, I. S., Heitor, M. V. and Santos, D., *3rd International Conference on Multiphase Flow (ICFM98)*, Lyon, France, (1998).
[5] El-Shanawany, M. S. and Lefebvre, A. H., *Journal of Energy*, 4: 184-189, (1980).
[6] Fernandez, V. G., Lavergne, G. and Berthoumien, P., *Atomization and Sprays*, 21: 1-16, (2011).
[7] Fernandez, V. G., Lavergne, G. and Berthoumien, P., *Atomization and Sprays*, 21: 17-21, (2011).
[8] Gepperth, S., Guildenbecher, D., Koch, R. and Bauer, H.-J., *ILASS Europe, 23rd Annual Conference on Liquid Atomization and Spray Systems*, Brno, Czech Republic, (2010).
[9] Kapulla, R., Tuchtenhagen, J., Müller, A., Dullenkopf, K. and Bauer, H.-J., *GALA Lasermethoden in der Strömungsmesstechnik*, (2008).
[10] Kline, S. and McClintock, F., *Mechanical Engineering*, 75: 3-8, (1953).
[11] Lefebvre, A. H., *Atomization and Sprays*, 10: 251-276, (2000).
[12] Müller, A., Koch, R., Bauer, H.-J., Hehle, M. and Schäfer, O., *ASME Turbo Expo 2006: Power for Land, Sea and Air*, GT2006-90432, (2006).
[13] Rizkalla, A. A. and Lefebvre, A. H., *Journal of Fluids Engineering*, 97: 316-320, (1975).
[14] Kim, K. S. and Kim, S. S., *Atomization and Sprays*, 4: 65-78, (1994).
[15] Lee, S. Y. and Kim, Y. D., *KSME International Journal*, 18: 879-894, (2004).
[16] White, F. M., *Viscous Fluid Flow*, New York: Mc Graw-Hill Book Co., (1991).